Research article

Journal of RAMAN SPECTROSCOPY

Received: 13 August 2013 Revised: 12 November 2013 Accepted: 20 November 2013 Published online in Wiley Online Library: 2 January 2014

(wileyonlinelibrary.com) DOI 10.1002/jrs.4429

Individual SERS substrate with core–satellite structure decorated in shrinkable hydrogel template for pesticide detection

Yiping Wu,[a,b,c] Pan Li,[c] Liangbao Yang[a,c]* and Jinhuai Liu[a,c]**

Individual Au@PNIPAM/Ag composite has been designed and fabricated as surface-enhanced Raman scattering (SERS) substrate in this paper. Because of the high porosity of the polymer shell and the driving force of the Au core to $Ag^{+}(H_2O)_n$ ($n = 1–4$) in aqueous solution, chemical reactions can be carried out while aggregation is completely avoided. Also, this makes the formation of vast and monodisperse Ag nanoparticles within PNIPAM and increases the colloidal stability. The Au cores with different sizes and the vast Ag nanoparticles then form core–satellite structures that can generate plasmon resonance. Moreover, this kind of individual Au@PNIPAM/Ag composite can be seen directly through Raman optical microscope, and uncertain effects on SERS signals resulting from variability of the configurations are minimized because these individual composite particles are relatively uniform. Importantly, the gaps between the Au and Ag nanoparticles can decrease because the PNIPAM shrinks from swollen to collapse state, so the substrate can also be used for inspecting pesticide residues accurately and rapidly. Copyright © 2014 John Wiley & Sons, Ltd.

Additional supporting information may be found in the online version of this article at the publisher's web site.

Keywords: individual; SERS substrate; polymer template; core–satellite structure; high reproducibility

Introduction

A variety of surface-enhanced Raman scattering (SERS) substrates have been developed in order to obtain sensitive and enhanced SERS signal.[1,2] Because the characteristic of structural parameters was accurately controlled, regular nanoparticle arrays and other nanofabricated SERS substrates have been widely used as SERS substrate with highly reproducible and large enhancement factors (EFs) 'by design'. Particularly, Raman EF as large as 10^8–10^{14} was observed.[3,4] However, the sub-nanometer control on the interspace between particles has to face the problem of poor structural reproducibility, which results in a wide distribution of EF values and unquantifiable/irreproducible SERS signals.[5] It is still difficult to fabricate well-controlled small gaps or complex geometries on the scale of a few nanometers to create efficient and abundant 'hot spots'.[6]

Individual nanoparticles, nanoscale junctions, and nanoaggregations have been intensively studied because the exact position of the hot spots can be conveniently located *in situ* by using an optical microscope during the SERS measurement rather than a scanning electron microscope or atomic force microscope after the SERS measurement and thus provide reliable reproducibility. For example, Liu *et al*. reported that individual particles could be clearly observed under dark-field illumination and SERS signal obtained on a single particle has high and extremely narrow distribution of EFs.[7] Yoon *et al*. prepared a SERS platform composed of a single metallic nanowire (NW) on a metallic film. Optical excitation of this sandwich nanostructure provides a line of SERS hot spots (a SERS hot line) at the gap between the NW and the film.[8] Goddard *et al*. demonstrated a high resolution spectral flow cytometer capable of acquiring Raman spectra of individual SERS tags at flow rates of hundreds of particles per second.[9] SERS-active substrates are generally geometry-controlled nanostructures and nanoparticle aggregates (often resulting from nonspecific aggregation) including dimeric structures in which the analyte is localized at a junction between the nanoparticles.[10,11] However, SERS-based single-molecule detection generally faces a problem with substrate structural reproducibility, as particle structure and interparticle distance can markedly affect Raman signals and constructing robust SERS-active nanostructures still remains challenging.[12] Recently, Gandra *et al*. reported a kind of core–satellite structures composed of shape-controlled plasmonic nanostructures. The in-built electromagnetic hot spots and Raman reporters of core–satellite structures make them excellent candidates for SERS probes.[13] So far, these core–satellite structures have also been achieved through either beam lithography or DNA-mediated assembly.[14–16]

On the other hand, hydrogel has been widely used as a carrier for the immobilization of metal nanoparticles combined with its unique properties (high level of water in its composition, and reversible volume changes). Such nanocomposite hydrogels have

* *Correspondence to: Liangbao Yang, Institute of Intelligent Machines, Chinese Academy of Science, Hefei 230031, China. E-mail: lbyang@iim.ac.cn*

** *Correspondence to: Jinhuai Liu, Institute of Intelligent Machines, Chinese Academy of Science, Hefei 230031, China. E-mail: jhliu@iim.ac.cn*

a *School of Chemistry and Chemical Engineering, Anhui University, Hefei 230039, China*

b *School of Chemistry and Chemical Engineering, Anqing Normal University, Anqing 246011, China*

c *Institute of Intelligent Machines, Chinese Academy of Sciences, Hefei 230031, China*

Journal of RAMAN SPECTROSCOPY

attracted intensive interest in many fields.[17–19] For example, the Liz-Marzan's group developed some approaches such as grafting polymers directly on the particles or *in situ* reduction of metal ions within the polymer made possible to increase the metal concentration and therefore to obtain composite materials with synergic properties that can be applied for optical sensing.[20–24] Our group has reported a strategy that allows one to finely tune the distance between Ag nanoparticles decorated on thermoresponsive microgels poly (*N*-isopropylacrylamide) (PNIPAM) to create vast 'hot spots' for electromagnetic enhancement. Dynamic gap (i.e. the interparticle distance) can be tuned easily because the microgel template undergoes a phase transition by changing the temperature.[25]

Herein, a simple and straightforward method to prepare individual core–satellite structure SERS substrate with dynamic gap was studied. Au nanoparticles cores with controllable sizes ranging from 20 to 110 nm were obtained through a seed-mediated growth. The shell is PNIPAM, which can generate *in situ* polymerization on the Au core surface without complicated functionalization. Importantly, the shell has been embodied with vast Ag nanoparticles that are significantly more efficient than gold as a plasmonic metal, and the Au–Ag nanoparticle also produces surface plasmon resonance. The big Au nanoparticle and the vast small Ag nanoparticles form a kind of core–satellites structure. Moreover, the Au@PNIPAM/Ag composite can be synthesized in aqueous solution, and it will shrink to half size of the original when drying, which would cause the nanoparticle gap to decrease and generate vast 'hot spot'.[26] This behavior arises from the loss of hydrogen bonding to amide groups (hydrophilic sites of –C O and –NH) in the hydrogel copolymer and leads to a collapse of the expanded structure. So it will be an excellent SERS substrate.

Experimental section

Materials

All chemicals used were analytical-reagent grade and used as received. Cetyltrimethylammonium bromide (CTAB), chloroauric acidtetrahydrate ($HAuCl_4.3H_2O$), trisodium citrate dehydrate (NaCt), silver nitrate ($AgNO_3$), sodium borohydride ($NaBH_4$), ascorbic acid (AA), *N*-isopropylacrylamide (NIPAM, 97%), glycine (98.5%), *N*, *N*′-methylenebisacrylamide (BIS), sumithion, *p*-aminothiophenol (4-ATP), and 2-2′-azobis (2-methylpropionamidine) dihydrochloride (AAPH) were purchased from Shanghai Chemical Reagent Ltd. Co. of China. All solutions were prepared using ultrapure water (resistance $> 18\,M\Omega\,cm^{-1}$).

Sample preparation

Au (d~20 nm)@PNIPAM-1 particles

Of Au nanoparticles (average diameter 20 nm), 10 ml were prepared as described elsewhere[27] by NaCt reduction and then diluted with 3.75 ml of a 0.2 M CTAB solution and water to 50 ml. The solution was purged with nitrogen (15 min) at 70 °C, followed by addition of NIPAM (0.1698 g) and BIS (0.0234 g). After 15 min, the nitrogen flow was removed, and the polymerization was initiated with the addition of AAPH (600 μl, 0.1 M). After 5–10 min, the wine-reddish mixture solution became turbid, and the reaction was allowed to proceed for 2 h at 70 °C. The reddish-white mixture was then allowed to cool down to room temperature under stirring. To remove small oligomers and unreacted monomers, the dispersion was centrifuged (10 min at 8000 rpm), and the precipitate was washed three times with milli-Q water. At last, they were redispersed in 10 ml of water.

Au (d~60 nm)@PNIPAM-2, Au (*d*~110 nm)@PNIPAM-3, and Au (*d*~150 nm)@PNIPAM-4 particles

The growth of the Au core was carried out following the method developed by Rodriguez-Fernandez *et al.*[27] Briefly, AA (0.1 M, 100 μl) solution was added into 18 ml of mixture of $HAuCl_4$ (2.5×10^{-4} M, 180 μl) and CTAB (0.2 M, 900 μl) at 25 °C, followed by addition of 4 ml seed solution (Au@PNIPAM-1) under magnetic stirring. After 30 min, the growth process was finished. The Au core size measured from transmission electron microscopy (TEM) was about 60 nm. Once again, using the Au@PNIPAM-2 as seeds, we obtained Au@PNIPAM-3. Using the Au@PNIPAM-3 as seeds, we obtained Au@PNIPAM-4. At last, they were redispersed in 10 ml of water.

Au@PNIPAM/Ag-(1–3) particles

The decorating of Au@PNIPAM-1 with Ag nanoparticles was carried out following the method. $AgNO_3$ (50 μl, 0.2 M) was added under mild magnetic stirring to 1 ml of Au@PNIPAM-1. The mixture was kept for 30 min at 25 °C to allow Ag^+ to get into the composites fully. Then, 50 μl of $NaBH_4$ (0.1 M) was added to the sample under vigorous magnetic stirring to promote the nucleation of Ag nanoparticles inside the PNIPAM. Silver growth was achieved by adding a mixture composed of CTAB (2.5 ml, 0.2 M), glycine at pH 9.5 (2.5 ml, 0.4 M), and $AgNO_3$ (400 μl, 0.2 M) to the previously treated Au@PNIPAM-1 solution. Then, 600 μl of AA 0.1 M was added under vigorous magnetic stirring, and the mixture was maintained at 25 °C for 30 min, followed by centrifugation (1000 rpm, 10 min) to remove excess AA and washing two times with water. At last, they were redispersed in 10 ml of water (i.e. Au@PNIPAM/Ag-1 particle). Using the same method, Au@PNIPAM-2 and Au@PNIPAM-3 were decorated with Ag nanoparticles, and we obtained Au@PNIPAM/Ag-2 and Au@PNIPAM/Ag-3 particles.

Samples detection

The SERS of 4-ATP were recorded. First, 1-ml aliquots of Au@PNIPAM/Ag-3 composites were stabilized at room temperature. Then, analyte was added to each nanoparticles suspension reaching final concentrations of 10^{-9} M. Of the corresponding suspension, 1 μl was cast on a silicon slide. After 30 s, the suspension did not flow, but the particles were still at wet state, and an individual composite particle was observed through Raman microscope. Then, this particle was excited with a 532-nm laser line and was collected at wet state. After 70 s, this particle was dry, and the same method was used to collect the SERS image here. The SERS detections of sumithion were carried out following the aforementioned method.

Characterization

The TEM images were obtained from a JEOL JEM-2010 instrument operated at 100 kV. Ultraviolet–visible (UV–vis) absorption spectra were collected on a Solidspec-3700 spectrophotometer. Raman spectra were collected from DXR Smart Raman spectra and were carried out on a LabRAM HR800 confocal microscope Raman system (Horiba Jobin Yvon). The microscope objective for laser illumination and signal collection was of long working

distance (8 mm) with 50 magnifications and a numerical aperture of 0.5. Integration times were provided as 2 s. The power at the sample was 0.2 mW.

Results and discussion

The formation of Au@PNIPAM/Ag composite was shown in Fig. 1. Here, we chose a simple method without complicated surface functionalization to synthesize Au@PNIPAM/Ag composite (see Fig. S1 in Supporting Information). As we know, cetyltrimethylammonium bromide (CTAB) solution can make the Au colloid stable and assist Au nanoparticle seed growth. The surface of Au nanoparticle can form admicelle because of the adsorption of a surfactant bilayer.[28] The next process is the solubilization of monomer [NIPAM and *N*,*N*′-methylenebisacrylamide (BIS)] into the admicelle; this phenomenon is called adsolubilization. The *in situ* polymerization of the monomer can generate when initiator 2-2′-azobis (2-methylpropionamidine) dihydrochloride (AAPH) is added into the aforementioned solution, so the coating of Au by PNIPAM gel completes. When washing of the treated Au@PNIPAM, much of the outer surfactant layer will be removed and the PNIPAM gels expose, then the growth of Au core in situ is under control.

The growth of Ag nanoparticles *in situ* on PNIPAM was due to the existence of driving force from Au core. Generally, metal ions always existed as $M^+(H_2O)_n$ ionic clusters in aqueous solution,[29] and there may be hydrogen bonds between H_2O of $M^+(H_2O)_n$ and amide bonds of the PNIPAM [Fig. 2(A)]. The PNIPAM microgels display a positive surface charge because of a cationic initiator (AAPH).[24] There is electrostatic repulsion between PNIPAM and $Ag^+(H_2O)_n$ ($n = 1$–4) [as shown in Fig. 2(B)]. Therefore, the $Ag^+(H_2O)_n$ in aqueous solution cannot easily enter into the porosity of the PNIPAM if not having a driving force from the outside. This has been demonstrated by our former study.[25]

Here, the Au core of Au@PNIPAM composite is negative surface charge because of the reduction of trisodium citrate dehydrate (NaCt), and it would have electrostatic attraction to the $Ag^+(H_2O)_n$ [Fig. 2(C)]. The driving force from Au core would drive $Ag^+(H_2O)_n$ to enter into the PNIPAM gel.

According to these, the significant aspect of this core–satellite structure is the Ag^+ entering into the porosity because of the electrostatic attraction from the Au core. It has been reported that spherical Au nanoparticles in a wide size range can be prepared in aqueous solutions of the cationic surfactant CTAB, through a seeded growth method in which an ionic precursor is catalytically reduced by AA, a mild reducing agent, on preformed Au seeds.[27] Moreover, using the Au (d~20 nm) @PNIPAM-1 particles [see Figs S2(A) and S4(A) in Supporting Information] as seeds, further growth steps of Au core carried out by reduction of $HAuCl_4$ with AA will increase the surface charge, which is a benefit to adsorbing more Ag^+ into the PNIPAM.[24] As a result, Au nanoparticles with average sizes of 60 nm [Au@PNIPAM-2, see Fig. S4(B) in Supporting Information] and 110 nm [Au@PNIPAM-3, as shown in Fig. 3(A)] were produced. Although the particles are rather faceted, and thus not perfectly spherical, the growth is very uniform up to almost 110 nm, without the formation of elongated particles. Au (d~150 nm) @PNIPAM-4 composite has also been studied as shown in Fig. S6 (Supporting Information). Original Au core and PNIPAM shell morphology has been destroyed, and the composites are not monodisperse.

To clearly understand the driving force of different sizes of Au core, in the next experiments, Au@PNIPAM-1, Au@PNIPAM-2, and Au@PNIPAM-3 were used as templates to grow Ag nanoparticles. The results show that the sizes of Au core play an impact on the corresponding Au@PNIPAM/Ag composite: The Ag nanoparticles in Au@PNIPAM/Ag-1 and Au@PNIPAM/Ag-2 are rare and not uniform [Fig. S4(C) and S4(D) in Supporting Information]. But Au (d~110 nm) @PNIPAM/Ag-3 composite is highly uniform. Figure 3 (B) shows the morphology of individual Au@PNIPAM/Ag-3 nanoparticles, and their sizes are about 900 nm. The Ag nanoparticles are relatively uniform, and their sizes are about 30 nm.

To examine the composition of the structures, Energy Dispersive X-ray (EDX) measurements were performed from two different positions of Au@PNIPAM/Ag-3 composite [as indicated by the red circles in Fig. 3(B)]. Figure 3(C) and 3(D) provides the representative spectra of the composites. In the case of the core position (i.e. the biggest nanoparticle), the characteristic peaks of Au and Ag are detected [Fig. 3(C)]. Peaks intensity due to Au has obviously more strength than that due to Ag, which demonstrated that the core of the core–satellite structure is Au nanoparticle. In contrast, the other position that avoids the biggest Au nanoparticle shows only characteristic peak of Ag [Fig. 3(D)].[30] The results of EDX patterns demonstrate further that the Au and the vast Ag nanoparticles formed core–satellite structures through this simple polymer template.

Although AA-reduced silver colloids have also negative surface charge, they are repelled by the Au core [Fig. 4(B)].[31] Herein, the PNIPAM has high porosity, which makes the vast Ag colloidal seeds stable. At the same time, the positive charges of PNIPAM microgels surface have electrostatic attraction to Ag nanoparticles with negative charge [Fig. 4(A)]. Under the balance of the two opposing force, the Au and Ag nanoparticles are distributed uniformly in PNIPAM gel while aggregation of nanoparticles is completely avoided. Such high and uniform coverage of Ag nanoparticles made the Au@PNIPAM/Ag substrate full of hot spots, which imparted superior SERS enhancement to the PNIPAM/Ag composites; thus, they could work as highly efficient SERS substrates.

The PNIPAM/Ag composite [see Fig. S3(B) in Supporting Information] also shows vast Ag nanoparticles, which are onside the entire surface of nanosphere template, but it cannot be observed directly through Raman microscope even at its swollen state because of its small size. Here, interestingly, individual particles [as indicated by the red circles in Fig. 5(B)] obtained by

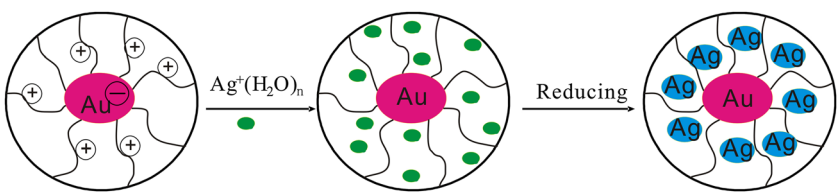

Figure 1. Schematic representation of formation mechanism of Au@PNIPAM/Ag composite.

Journal of RAMAN SPECTROSCOPY

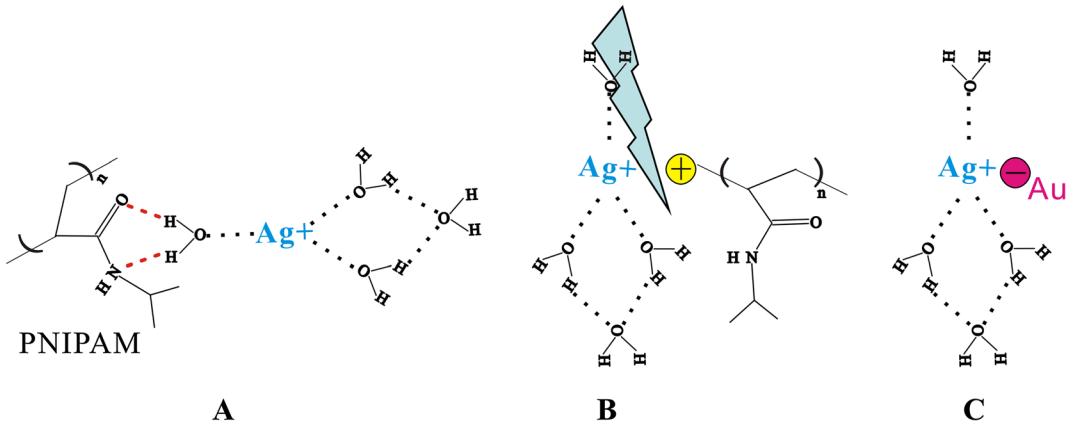

Figure 2. Schematic representation of the possible interactions between Au@PNIPAM composite and Ag^{+} $(H_2O)_4$: (A) possible hydrogen-bonding interaction, (B) electrostatic repulsive force between the cation–cation pairs, and (C) electrostatic attractive force through the anion–cation pair.

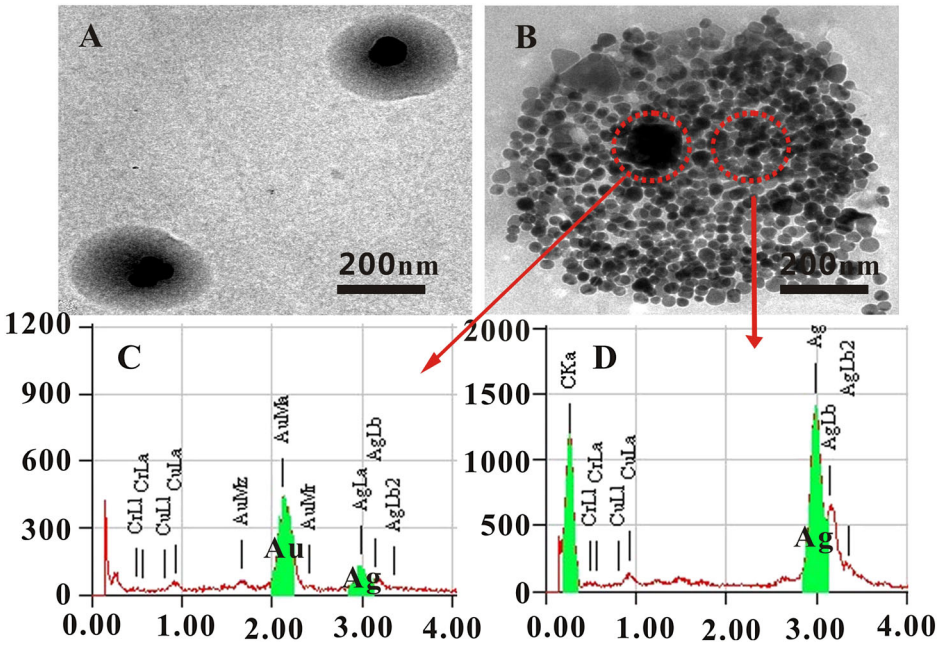

Figure 3. TEM images of Au@PNIPAM-3 (A) and Au@PNIPAM/Ag-3 (B) composites, and EDX pattern of Au@PNIPAM/Ag-3 composite within two different regions: (C) and (D), respectively.

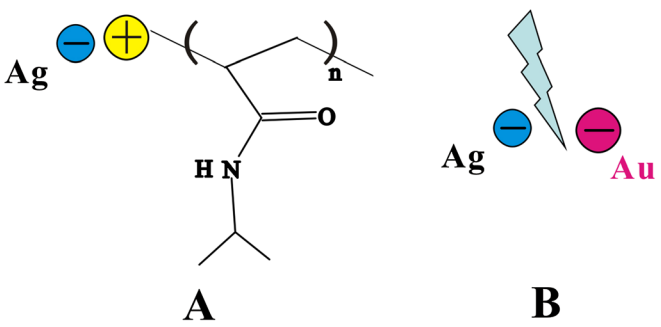

Figure 4. Schematic representation of the possible interactions between Au@PNIPAM composite and Ag nanoparticle: (A) electrostatic attractive force between Ag nanoparticle and PNIPAM gel, and (B) electrostatic repulsive force between Au and Ag nanoparticles.

casting the dilute composite solutions onto a silicon substrate could be clearly observed under Raman microscope when at their swollen and shrunken state [Fig. 5(B)] because of their micrometer sizes. It is possible to obtain high repeatable image through individual particle.

The optical enhancing properties of the Au@PNIPAM/Ag composites were tested using *p*-aminothiophenol (4-ATP), which SERS spectrum is well established.[32,33] The substrate has no impacts on the detected molecules, and the EF provided by Au@PNIPAM/Ag-3 is higher than that from Au@PNIPAM/Ag-1 and Au@PNIPAM/Ag-2 particles (see Figs S7 and S8 in Supporting Information), which is consistent with the densest 'hot spot' of individual Au@PNIPAM/Ag-3 particle than that of Au@PNIPAM/Ag-1 and Au@PNIPAM/Ag-2 particles as shown in Figs 3(B) and S4 (Supporting Information). Therefore, in all the experiments

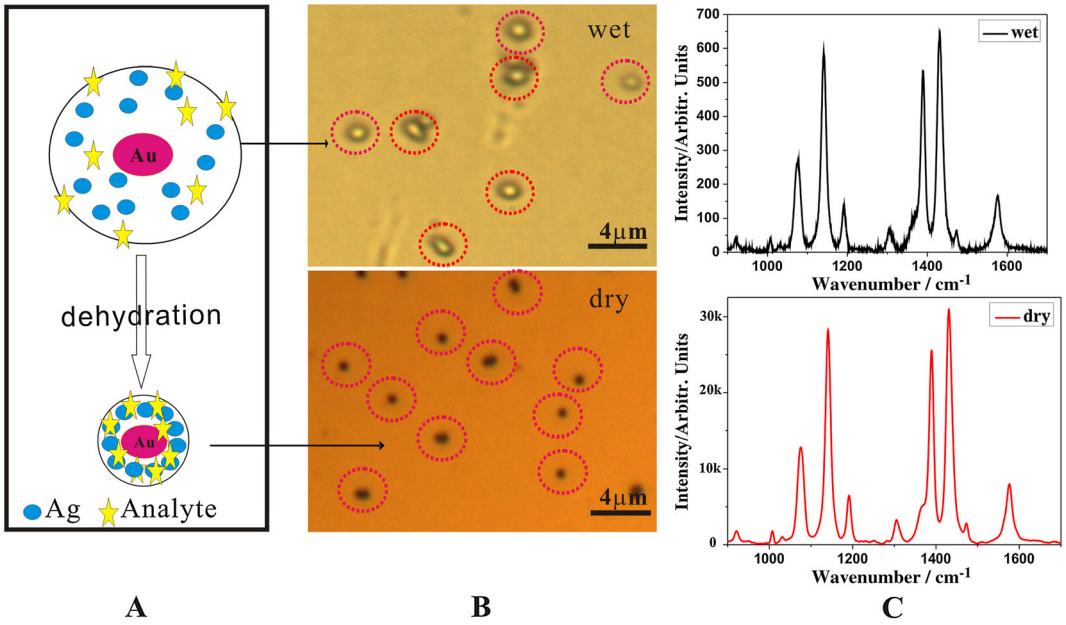

Figure 5. Schematic illustration of the changes of the composite from (top) swollen state to (bottom) shrunken state due to dehydration (A), optical image of Au@PNIPAM/Ag-3 under Raman microscope (B), and SERS spectra of 4-ATP (10^{-9} M) obtained from the individual Au@PNIPAM/Ag-3 nanoparticle (C) at (top) wet and (bottom) dry state, respectively.

described later for the design of other analytical applications of these materials, only the Au@PNIPAM/Ag-3 particles were employed. The UV–vis spectrum of Au@PNIPAM/Ag-3 composite shows a plasmon band at (403 ± 2) nm, which is consistent with the same size Ag NPs (Fig. S9 in Supporting Information), so 532 nm laser line was only chosen.

As we know, PNIPAM has been extensively studied in regard to its well-known phase behavior in aqueous solutions, which has the sharpest transition of the class of thermosensitive alkylacrylamide polymers. Dehydration takes place in the PNIPAM when it transforms from wet state to dry state, which results in the subsequent aggregation of the PNIPAM chain and leads to the shrinking of the hydrogel. This also can be seen clearly under Raman microscope: The size of the composite is smaller at dry state than that at its wet state [Fig. 5(B)]. SERS measurements at the two states are also obtained. The Raman band from individual wet substrate is weak [top of Fig. 5 (C)]. It is remarkable that an increasing SERS signal about two orders of magnitude will be get when the substrate is dry [bottom of Fig. 5(C)]. Actual Raman intensity for Raman spectrum with dry condition would decrease slightly,[34] but here it is not. It is clear that exceeding small structures and gaps (<10 nm) are required to generate the 'hot spots' typically associated with high SERS activity.[12] The collapse of the gel makes the nanoparticles approach each other and generate highly active hot spots; on the other hand, once the substrate is dehydrated, the material collapses, trapping the analytes within the hot spots generated by the close proximity of the plasmonic nanoparticles.[23] These changes lead to an increasing SERS signal, which is consistent to our previous study about PNIPAM hydrogel.[25]

Many SERS-active nanostructures have been investigated, but they suffer from poor reproducibility of the SERS-active sites, and the wide distribution of their EF values, which result in an inhomogenous SERS signal. To our convenient, the individual composite is so big that it can be seen directly in microscope. So long as we use the laser illuminating any individual composite, strong SERS signal will be obtained. To investigate the dependence of the SERS enhancement on each individual composite, the characteristic peaks of 4-ATP from a single composite nanosphere have been clearly recorded. Each individual particle is chosen at its dry state [as indicated by the red circles in the bottom of Fig. 5(B)] and obtains the SERS image spectra as shown in Fig. 6(A). Every particle could generate the detectable SERS signals. The main Raman vibrations at 1430, 1388, and 1140 cm^{-1} from 30 individual particles are obviously enhanced at all spots, indicating excellent SERS activity and reproducibility. To obtain statistically meaningful results, the relative standard deviation (RSD) of the Raman intensity of the carbon skeleton stretching modes is calculated. Figure 6 (B)–6(D) shows that the RSDs of the Raman peaks at 1430, 1140, and 1388 cm^{-1} are 0.1184, 0.1382, and 0.1206, respectively, which clearly reveals the high reproducibility of the substrate. The high reproducibility of this system can be explained by the following interpretation: The vast Ag nanoparticles distribute uniformly around the big Au core because of the balance of different electrostatic forces during the formation of composite; on the other hand, the gap of the Au and Ag could be decreased obviously because of the hydrogel template transformed from swollen state to shrunk state. These are consistent with the TEM image of individual Au@PNIPAM/Ag-3 composite, as shown in Fig. 3(B), which is highly uniform.[35,36]

Recently, environmental problems have drawn more and more attention to the organic pollutants related to wastewater and polluted food. SERS obtained from individual Au@PNIPAM/Ag-3 particles at their dry states can also be used for inspecting pesticide residues accurately and rapidly, such as the organophosphate pesticide sumithion. SERS spectra of sumithion are collected by varying their concentration from 10^{-5} to 10^{-9} M.

Journal of RAMAN SPECTROSCOPY

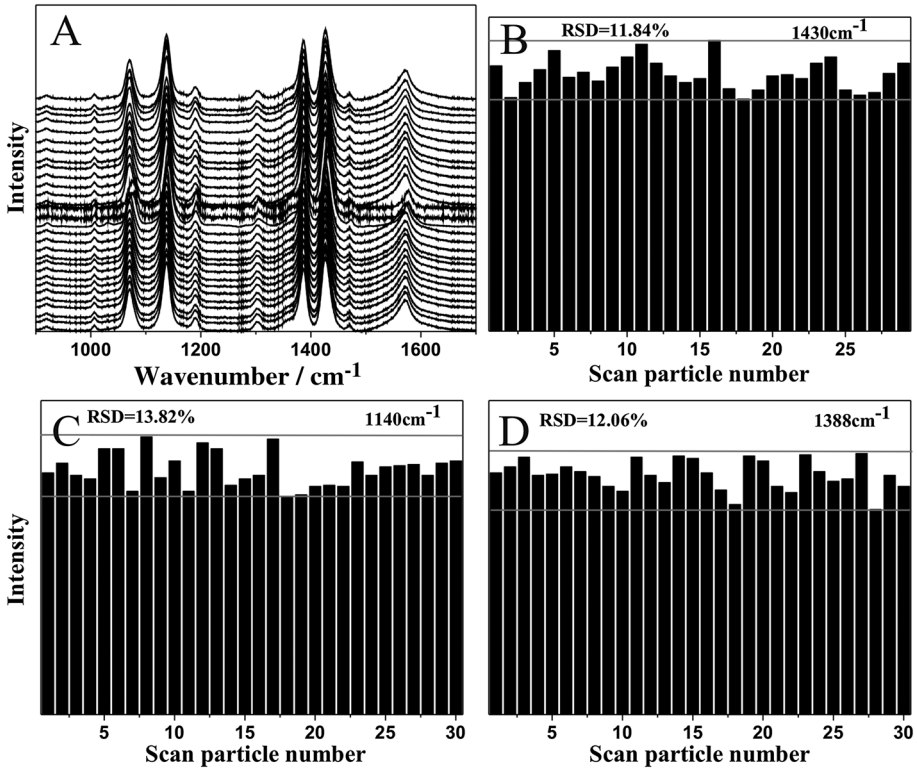

Figure 6. A series of SERS spectra of 10^{-9} M 4-ATP molecules collected on 30 randomly selected individual Au@PNIPAM/Ag particles at their dry state (A) and the relative standard deviation (RSD) of the integrated Raman intensity (B), (C), and (D).

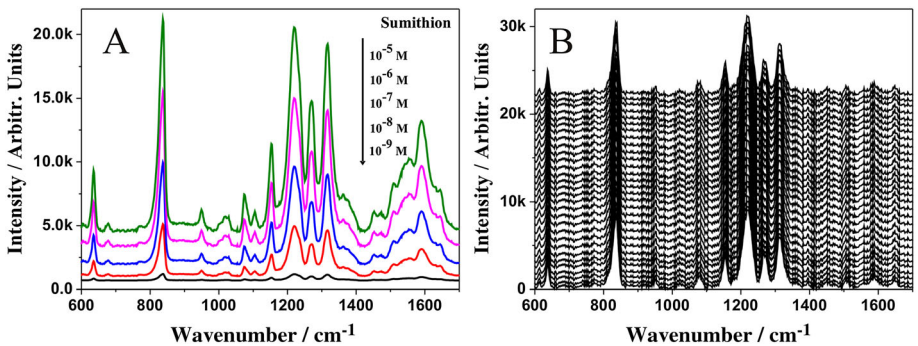

Figure 7. SERS spectra obtained from different concentrations of sumithion using individual Au@PNIPAM/Ag-3 particle: from 10^{-5} to 10^{-9} M (A). A series of SERS spectra of 10^{-8} M sumithion molecules collected on 30 randomly selected individual Au@PNIPAM/Ag-3 particles (B).

As shown in Fig. 7(A), 10^{-9} M sumithion can be still detected using this individual substrate. Figure 7(B) illustrates a series of SERS spectra of 10^{-8} M sumithion molecules collected on 30 randomly selected individual Au@PNIPAM/Ag-3 particles at their dry state. Figure S10 (Supporting Information) shows that the RSDs of the Raman peaks at 635 and 837 cm^{-1} are 0.1281 and 0.1306, respectively, which clearly reveals the high reproducibility of the substrate.

Conclusions

A new stepwise strategy has been developed for the assembling of gold and silver nanoparticles by PNIPAM template for SERS application. These novel stimuli-responsive systems offer obvious advantage: The growth of Au core *in situ* is controllable, and Ag nanoparticles are distributed uniformly in PNIPAM gel under the balance of different forces. The colloidal stability of the particles is improved without any complicated surface functionalization; the position of hot spots can be conveniently located *in situ* by using an optical microscope during the SERS measurement. An increasing SERS signal about two orders of magnitude due to an increased near-field coupling between the Au and Ag nanoparticles accompanying the changing conformational of the hydrogel can be get. The RSDs of the integrated Raman intensity from different concentrations of 4-ATP and sumithion are both less than 15%, which demonstrate the high reproducibility of SERS signal from every individual composite substrate.

Acknowledgements

This work was supported by the National Basic Research Program of China (2011CB933700), the National Instrumentation Program of China (2011YQ0301241001 and 2011YQ0301241101), the Key Projects of National Science Foundation of China (21271136), and the Graduate Students Innovative Program of Anhui University (01001770–10117700061).

References

[1] L. B. Yang, L. A. Ma, G. Y. Chen, J. H. Liu, Z. Q. Tian, *Chem-Eur. J.* **2010**, *16*, 12683.
[2] X. H. Li, G. Y. Chen, L. B. Yang, Z. Jin, J. H. Liu, *Adv. Funct. Mater.* **2010**, *20*, 2815.
[3] H. L. Liu, Y. D. Sun, Z. Jin, L. B. Yang, J. H. Liu, *Chem. Sci.* **2013**, *4*, 3490.
[4] Q. Q. Ding, Y. M. Ma, Y. J. Ye, L. B. Yang, J. H. Liu, *J. Raman. Spectrosc.* **2013**, *44*, 987.
[5] Y. Fang, N. H. Seong, D. D. Dlott, *Science* **2008**, *321*, 388.
[6] J. X. Fang, S. Y. Du, S. Lebedkin, Z. Y. Li, R. Kruk, M. Kappes, H. Hahn, *Nano Lett.* **2010**, *10*, 5006.
[7] R. Y. Liu, B. H. Liu, G. J. Guan, C. L. Jiang, Z. P. Zhang, *Chem. Commun.* **2012**, *48*, 9421.
[8] I. Yoon, T. Kang, W. Choi, J. Kim, Y. Yoo, S. W. Joo, Q. H. Park, H. Ihee, B. Kim, *J. Am. Chem. Soc.* **2009**, *131*, 758.
[9] G. Goddard, L. O. Brown, R. Habbersett, C. I. Brady, J. C. Martin, S. W. Graves, J. P. Freyer, S. K. Doorn, *J. Am. Chem. Soc.* **2010**, *132*, 6081.
[10] Y. J. Ye, H. L. Liu, L. B. Yang, J. H. Liu, *Nanoscale* **2012**, *4*, 6442.
[11] H. L. Liu, L. B. Yang, H. W. Ma, Z. M. Qi, J. H. Liu, *Chem. Commun.* **2011**, *47*, 9360.
[12] D. K. Lim, K. S. Jeon, H. M. Kim, J. M. Nam, Y. D. Suh, *Nat. Mater.* **2010**, *9*, 60.
[13] N. Gandra, A. Abbas, L. M. Tian, S. Singamaneni, *Nano Lett.* **2012**, *12*, 2645.
[14] L. G. Xu, H. Kuang, C. L. Xu, W. Ma, L. B. Wang, N. A. Kotov, *J. Am. Chem. Soc.* **2012**, *134*, 1699.
[15] X. Y. Xu, N. L. Rosi, Y. H. Wang, F. W. Huo, C. A. Mirkin, *J. Am. Chem. Soc.* **2006**, *128*, 9286.
[16] J. A. Fan, Y. He, K. Bao, C. H. Wu, J. M. Bao, N. B. Schade, V. N. Manoharan, G. Shvets, P. Nordlander, D. R. Liu, F. Capasso, *Nano Lett.* **2011**, *11*, 4859.
[17] M. Mueller, M. Tebbe, D. V. Andreeva, M. Karg, R. A. Alvarez-Puebla, N. Pazos-Perez, A. Fery, *Langmuir* **2012**, *28*, 9168.
[18] P. Liu, J. G. Sun, J. H. Huang, R. Peng, J. Tang, J. D. Ding, *Nanoscale* **2010**, *2*, 122.
[19] A. Lee, G. F. S. Andrade, A. Ahmed, M. L. Souza, N. Coombs, E. Tumarkin, K. Liu, R. Gordon, A. G. Brolo, E. Kumacheva, *J. Am. Chem. Soc.* **2011**, *133*, 7563.
[20] R. Contreras-Caceres, A. Sanchez-Iglesias, M. Karg, I. Pastoriza-Santos, J. Perez-Juste, J. Pacifico, T. Hellweg, A. Fernandez-Barbero, L. M. Liz-Marzan, *Adv. Mater.* **2008**, *20*, 1666.
[21] R. A. Alvarez-Puebla, R. Contreras-Caceres, I. Pastoriza-Santos, J. Perez-Juste, L. M. Liz-Marzan, *Angew. Chem. Int. Ed.* **2009**, *48*, 138.
[22] R. Contreras-Caceres, S. Abade-Cela, P. Guardia-Giros, A. Fernandez-Barbero, J. Perez-Juste, R. A. Alvarez-Puebla, L. M. Liz-Marzan, *Langmuir* **2011**, *27*, 4520.
[23] R. A. Alvarez-Puebla, L. M. Liz-Marzan, *Chem. Soc. Rev.* **2012**, *41*, 43.
[24] R. Contreras-Caceres, I. Pastoriza-Santos, R. A. Alvarez-Puebla, J. Perez-Juste, A. Fernandez-Barbero, L. M. Liz-Marzan, *Chem-Eur. J.* **2010**, *16*, 9462.
[25] Y. P. Wu, F. Zhou, L. B. Yang, J. H. Liu, *Chem. Commun.* **2013**, *49*, 5025.
[26] J. Wahrmund, J. W. Kim, L. Y. Chu, C. J. Wang, Y. Li, A. Fernandez-Nieves, D. A. Weitz, A. Krokhin, Z. B. Hu, *Macromolecules* **2009**, *42*, 9357.
[27] J. Rodriguez-Fernandez, J. Perez-Juste, F. J. G. de Abajo, L. M. Liz-Marzan, *Langmuir* **2006**, *22*, 7007.
[28] J. H. Ohaver, J. H. Harwell, E. A. Orear, L. J. Snodgrass, W. H. Waddell, *Langmuir* **1994**, *10*, 2588.
[29] D. Feller, E. D. Glendening, W. A. de Jong, *J. Chem. Phys.* **1999**, *110*, 1475.
[30] J. F. Huang, S. Vongehr, S. C. Tang, H. M. Lu, J. C. Shen, X. K. Meng, *Langmuir* **2009**, *25*, 11890.
[31] K. Qian, H. L. Liu, L. B. Yang, J. H. Liu, *Nanoscale* **2012**, *4*, 6449.
[32] G. K. Liu, J. Hu, P. C. Zheng, G. L. Shen, J. H. Jiang, R. Q. Yu, Y. Cui, B. Ren, *J. Phys. Chem. C* **2008**, *112*, 6499.
[33] R. T. Hill, J. J. Mock, Y. Urzhumov, D. S. Sebba, S. J. Oldenburg, S. Y. Chen, A. A. Lazarides, A. Chilkoti, D. R. Smith, *Nano Lett.* **2010**, *10*, 4150.
[34] L. B. Yang, H. L. Liu, Y. M. Ma, J. H. Liu, *Analyst* **2012**, *137*, 1547.
[35] H. B. Tang, G. W. Meng, Q. Huang, Z. Zhang, Z. L. Huang, C. H. Zhu, *Adv. Funct. Mater.* **2012**, *22*, 218.
[36] C. H. Zhu, Z. B. Hai, C. H. Cui, H. H. Li, J. F. Chen, S. H. Yu, *Small* **2012**, *8*, 930.

Supporting information

Additional supporting information may be found in the online version of this article at the publisher's web site.